Available online at www.sciencedirect.com
ScienceDirect
Journal of Power Sources 175 (2008) 891–896
JOURNAL OF POWER SOURCES
www.elsevier.com/locate/jpowsour

Short communication

$Li_{1+x}FePO_4$ ($0 \leq x \leq 3$) as anode material for lithium ion batteries: From *ab initio* studies

C.Y. Ouyang [a,b,d,*], S.Q. Shi [a], Q. Fang [c], M.S. Lei [d]

[a] *Department of Physics, Center for Optoelectronics Materials and Devices, Zhejiang Sci-Tech University, Hangzhou 310018, China*
[b] *Institut Romand de Recherche Num'erique en Physique des Mat'eriaux (IRRMA), Ecole Polytechnique Fédéral de Lausanne (EPFL), CH-1015 Lausanne, Switzerland*
[c] *Department of electronics, Jiangxi University of Finance and Economy, Nanchang 330013, China*
[d] *Department of Physics, Jiangxi Normal University, Nanchang 330027, China*

Received 3 August 2007; received in revised form 25 September 2007; accepted 29 September 2007
Available online 13 October 2007

Abstract

$Li_{1+x}FePO_4$ ($0 \leq x \leq 3$) as anode material for lithium ion batteries has been studied using *ab initio* calculations. Results show that large amount of lithium ions can be intercalated into $LiFePO_4$ host. The structure changes continuously when the first two Moles of lithium ions ($x \leq 2$) are intercalated into the $LiFePO_4$ host, accompanied by large volume expansion (37.4% and 25.4% for the first and second Mole). The final product of Li_3FePO_4 possesses a stable chained structure, which is favorable for storing even more lithium. In the same time, lithium ion diffuses in a three-dimension pathway within the chained structure. The unit cell volume increases only by 4.9% from Li_3FePO_4 to Li_4FePO_4, and the chained structure keeps unchanged.

Keywords: $LiFePO_4$; Anodes; *Ab initio* calculations; Intercalation; Charge distribution; Migration energy barrier

1. Introduction

The phospho-olivine $LiFePO_4$ has been extensively studied as cathode material for lithium ion batteries since the pioneering work by Goodenough and co-workers [1]. With advantages like high-energy density, low cost and good environmental compatibility, it has attracted great attention from the standpoint of both academy and industry.

However, the intrinsic low electronic and ionic conductivity of this material, which results in rather poor rate performance during cycling, is the major problem that inhibits its wide application in lithium ion batteries industry. Many studies have been done to improve the dynamic properties. It is shown that the electronic conductivity of $LiFePO_4$ could be largely improved through Li site doping [2,3], but the dopant cations at the Li sites might block the lithium one-dimensional diffusion pathway [4,5]. Numerous basic researches have also been carried out to understand both electron transport mechanism and lithium ion transport process during cycling [6,7]. Simultaneously, various studies have also been concentrated to improve the rate performance via decreasing the particle size or improving electronic contact [8,9]. Although many efforts have devoted to improve the rate performance, it is still an open difficulty to both academic and industrial.

Recently, Kalaiselvi et al. [10] have successfully shown that $LiFePO_4$ compound can be employed as anode material for rechargeable lithium batteries. The reversible capacity of about 300 mAh g^{-1} (after 20 cycles of charge/discharge) of $LiFePO_4$ anode indicates that ~2 lithium ions can be reversibly inserted into one $LiFePO_4$ formula, and becomes Li_3FePO_4. Later, the capacity of $LiFePO_4$ as anode material is further improved by doping with small amount of Cu or Sn at Fe sites [11]. The cycling capacity of the doped $LiFePO_4$ as anode material is enhanced to ~400 mAh g^{-1}, indicating that even more lithium ions can be reversibly stored in $Li_{1+x}FePO_4$ host. Although it has been shown that $LiFePO_4$ as anode possesses very good capacity and cycling performance, the lithium

* Corresponding author at: Department of Physics, Zhejiang Sci-Tech University, Hangzhou 310018, China. Tel.: +86 571 86434295.
E-mail addresses: chuying.ouyang@epfl.ch (C.Y. Ouyang), siqishi@zstu.edu.cn (S.Q. Shi).

0378-7753/$ – see front matter © 2007 Elsevier B.V. All rights reserved.
doi:10.1016/j.jpowsour.2007.09.116

storage mechanism behind the performance is not identified by the authors. For example, structural transition and change of Fe valence state during lithium intercalation process are not studied, which are obviously important for understanding of the lithium storage mechanism.

In the present work, we are going to investigate the basic physical and chemical problems of $LiFePO_4$ as anode material for lithium ion batteries from theoretical aspect of view, namely from density functional theory (DFT)-based *ab initio* calculations. The structural and electronic properties, charge transfer, lithium diffusion upon lithium intercalation are studied in detail.

2. Computational details

We have performed the DFT-based *ab initio* calculations using DACAPO code [12]. This code solves the Kohn–Sham equations within the pseudopotential approximation whereby the electrons are described in the generalized gradient approximation (GGA) [13]. The valence and core interactions are described by the Vanderbilt pseudopotentials [14]. The valence electrons wave functions and the augmented electron density are expanded in a plane wave basis sets with cutoff energies of 25 and 140 Ry, respectively. The Perdew–Wang exchange-correlation functional (PW91) [15] is used for the calculation of the electron exchange correlation energy.

$LiFePO_4$ has ordered olivine structure (space group *Pnma*), with lattice constants of $a = 10.334$ Å, $b = 6.0105$ Å, $c = 4.732$ Å [1]. The unit cell contains 4 $LiFePO_4$ formulas, including 28 atoms in all. For structural relaxation and total energy calculations, Monkhorst–Pack scheme [16] $3 \times 5 \times 7$ k points sampling is used for the integration in the irreducible Brillouin zone.

The migration of lithium ions are simulated with nudged elastic band (NEB) method [17,18]. The migration energy barriers are calculated within a dilute vacancy situation, with only one Li vacancy and otherwise all occupied Li atoms in the unit cell. As the NEB calculations are computational expensive, only gamma point is used for the NEB calculations.

Table 1
Lattice constant (in Å), unit cell volume V (in Å^3), magnetic moment of Fe atom MOM (in μ_B), and total energy difference ΔE (in eV per unit cell) of $FePO_4$ and $LiFePO_4$

	a	b	c	V	MOM	ΔE
$FePO_4$						
Non-spin	9.719	5.731	4.720	262.90	–	Reference
FM	10.009	5.980	4.856	290.65	4.02	−4.77
AFM	10.022	6.021	4.850	292.67	3.93	−5.53
$LiFePO_4$						
Non-spin	10.290	5.982	4.673	287.65	–	Reference
FM	10.651	6.206	4.817	318.36	3.55	−5.22
AFM	10.627	6.187	4.800	315.61	3.51	−5.38

ΔE is calculated with non-spin-polarized total energy as reference.

3. Crystal structure upon lithium intercalation

In the present work, we first optimized the theoretical equilibrium lattice constant of $FePO_4$ and $LiFePO_4$. The results are listed in Table 1. The theoretical lattice constants for the spin-polarized calculations are larger than the non-spin-polarized one. From comparing the total energy of the system under different magnetic configurations, we conclude that the bulk spin configuration is antiferromagnetic (AFM), in agreement with the results in Ref. [19]. For the AFM configuration, the unit cell volume of $FePO_4$ increases by about 7.8% after lithium ions are intercalated to become $LiFePO_4$.

Fig. 1a shows schematically the crystal structure of $LiFePO_4$. Within the unit cell, four Li atoms take the 4*a* positions while Fe and P atoms occupy part of the 4*c* positions and O atoms occupy part of 4*c* and 8*d* positions [1,20]. From the crystal structure, we can see that there are a lot of vacant sites available for lithium storage, including 4*b*, 4*c*, and 8*d* sites. When more lithium atoms

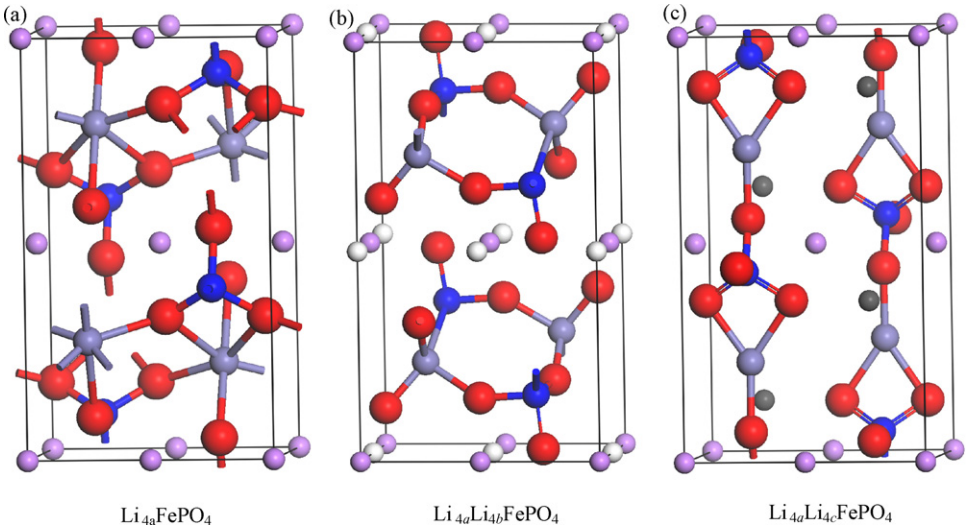

Fig. 1. Schematic view of the atomic structures of (a) $LiFePO_4$, (b) $Li_{4a}Li_{4b}FePO_4$, and (c) $Li_{4a}Li_{4c}FePO_4$. The largest red spheres are the O atoms, the middle sized spheres indicate the Fe (grey) and P (green) atoms, and the smallest spheres are lithium atoms, with purples color at the 4*a* sites, white at 4*b* sites, and grey at 4*c* sites. (For interpretation of the references to color in this figure legend, the reader is referred to the web version of the article.)

Table 2
Lattice constant (in Å), unit cell volume V (in Å^3), magnetic moment of Fe atom MOM (in μ_B), and total energy difference ΔE (in eV per unit cell) of Li_2FePO_4 optimized for Li occupy 4*c* and 4*b* sites

	a	*b*	*c*	*V*	MOM	ΔE
$Li_{4a}Li_{4b}FePO_4$						
Non-spin	12.027	6.430	4.923	380.69	–	Reference
FM	12.194	6.755	5.077	418.20	3.79	−8.94
AFM	12.340	6.966	5.118	439.94	3.75	−9.78
$Li_{4a}Li_{4c}FePO_4$						
Non-spin	11.905	6.558	5.135	400.93	–	−0.17
FM	11.960	6.890	5.246	432.31	2.99	−11.41
AFM	11.932	6.920	5.252	433.66	3.03	−11.71

ΔE is calculated with non-spin-polarized $Li_{4a}Li_{4b}FePO_4$ as reference.

are inserted into the $LiFePO_4$ lattice, we first need to know which site will be taken by these lithium atoms. 4*b* or 4*c* sites are the first choice. From the symmetry of crystal, the fractional coordinate of one 4*b* site is (0, 0, 0.5). However, for the 4*c* sites, only the *y*-coordinate is fixed to be 0.25, the *x*- and *z*-coordinates are flexible.

To simulate the structure of Li_2FePO_4, which is formed by intercalation additional four lithium atoms in one $LiFePO_4$ unit cell, we try to place these additional lithium atoms into either 4*b* or 4*c* sites, and the unit cells are denoted as $Li_{4a}Li_{4b}FePO_4$ and $Li_{4a}Li_{4c}FePO_4$, respectively. The calculated results are listed in Table 2. From the calculated total energy, we find out that the optimized bulk magnetic configuration of both $Li_{4a}Li_{4b}FePO_4$ and $Li_{4a}Li_{4c}FePO_4$ are antiferromagnetic. The total energy of the unit cell for lithium atoms at the 4*c* sites is about 2 eV lower than that with lithium taking the 4*b* sites. This indicates that the 4*c* sites are more favorable for lithium storage at the initial stage of lithium intercalation process. However, in both cases we observed a very large lattice expansion from $LiFePO_4$ to Li_2FePO_4. For the energetically most favorable AFM $Li_{4a}Li_{4c}FePO_4$ configuration, the volume of the unit cell increases about 37.4%, from 315.61 Å^3 to 433.66 Å^3. This is not favorable to the stability of the material during the intercalation process.

Presented in Fig. 1b and c are the optimized atomic structures of Li_2FePO_4 with AFM spin configuration. In the case of $LiFePO_4$, the FeO_6 octahedra and PO_4 tetrahedra are connected with shared edges and corners, and the crystal is compactly organized in three-dimensions [1], which ensure the structure to be very stable. However, in the case of Li_2FePO_4, either $Li_{4a}Li_{4b}FePO_4$ or $Li_{4a}Li_{4c}FePO_4$, the structure is quite loose, and the unit cell volume is much larger than that of $LiFePO_4$, as discussed above. In $Li_{4a}Li_{4b}FePO_4$, FeO_6 octahedra structures are transformed into tetrahedra, coordinated with one P and three O atoms. PO_4 tetrahedra structures are also changed, with P and Fe atoms directly coordinated. Due to these changes, the unit cell is organized in two rings. Each ring is formed with two P-tetrahedra and two Fe-tetrahedra. The structure is formed with these cluster rings. For each ring structure, the unshared (one-coordinated) O atoms are stretched into lithium layers, providing certain electron affinity and stabilizing those lithium atoms. In $Li_{4a}Li_{4c}FePO_4$, the FeO_6 octahedral structures also disappeared. The PO_4 tetrahedra structures are chained along *a*-direction. Those tetrahedra are connected to each other with Fe atoms, which are bonded by three O atoms and the FeO_3 structure is arranged within a plane.

In both $Li_{4a}Li_{4b}FePO_4$ and $Li_{4a}Li_{4c}FePO_4$, the crystal structure is substantially changed. The unit cell volume is largely increased and the structure becomes relatively loosen and unstable. As for electrode material for lithium batteries, this is obviously unfavorable for the cycling performance. However, the loose structure provides large space for lithium storage, which enables the high capacity as electrode material.

Fig. 2 shows the optimized atomic structures of Li_3FePO_4 with AFM spin ordering, which is also the energetically most favorable configuration, as shown in Table 3. By contrast with the structures of $LiFePO_4$ and Li_2FePO_4, the structure of the material and symmetry of the atoms are completely different. The structure of Li_3FePO_4 is constructed with quasi-one-dimensional chains along the *z*-axis direction. The chain structure is formed in a zigzag way by alternative Fe and O atoms, with one PO_3 group bonded to each Fe atom along the chain. Within the chained structure, the atoms are orga-

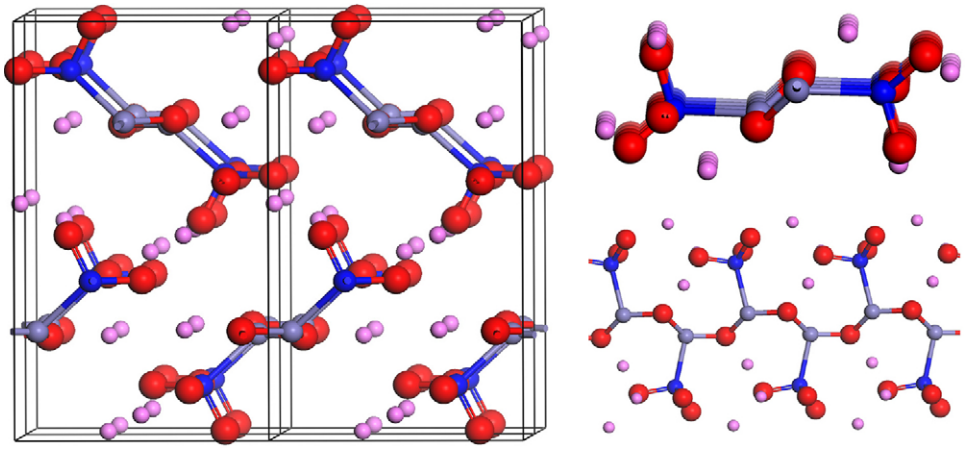

Fig. 2. Atomic structures of Li_3FePO_4 (left) and the chained structures in the crystal viewing from different direction (right). The size and color scheme for different atoms are the same as in Fig. 1. (For interpretation of the references to color in this figure legend, the reader is referred to the web version of the article.)

Table 3
Lattice constant (in Å), unit cell volume V (in Å^3), magnetic moment of Fe atom MOM (in μ_B), and total energy difference ΔE (in eV per unit cell) of Li_3FePO_4 and Li_3FePO_4

	a	b	c	V	MOM	ΔE
Li_3FePO_4						
Non-spin	12.884	7.605	5.364	525.21	–	Reference
FM	13.015	7.593	5.421	435.74	0.98	−0.54
AFM	12.995	7.657	5.468	544.01	2.66	−2.25
Li_4FePO_4						
AFM	13.372	7.646	5.584	570.90	2.52	–

ΔE is calculated with non-spin-polarized total energy as reference.

nized compactly, while the connection between each chain is quite loose. To form this structure, large volume expansion also required (from Li_2FePO_4 to Li_3FePO_4, the unit cell volume increased 25.4%), as shown in Tables 2 and 3. With such a structure, lithium atoms have very good mobility, which will be discussed in details in the following section. Li atoms are regularly distributed along the chained structure, stabilized by the electrostatic attraction from the PO_3 groups. The PO_3 groups are quite separated, which provide even more space for lithium storage.

Recent experiments shown that lithiation of transition metal oxides leads to formation of M/Li_2O nanocomposite, accomanied by large volume expansions, and after lithium is electrochemically removed out from the nanocomposite, the remaining of the nanocomposite is still in nano-sized metal oxide particles and is used for subsequent cycles [21–23]. In the case of lithiation of $LiFePO_4$ compound, our results show that a quasi-one-dimensional FeO–PO_3 chained structure is formed, which also provides good media for lithium storage. To verify this, we added more lithium in the unit cell of this structure, and the chemical composition becomes Li_4FePO_4. As expected, the chained structure is not changed in Li_4FePO_4, with 16 Li atoms in the unit cell, as shown in Fig. 3. These Li atoms are distributed around the chained structure, which ensures that lattice constants do not change much upon Li intercalation. As it is shown in Table 3, the unit cell volume increases only 4.9% from Li_3FePO_4 chained structure to Li_4FePO_4.

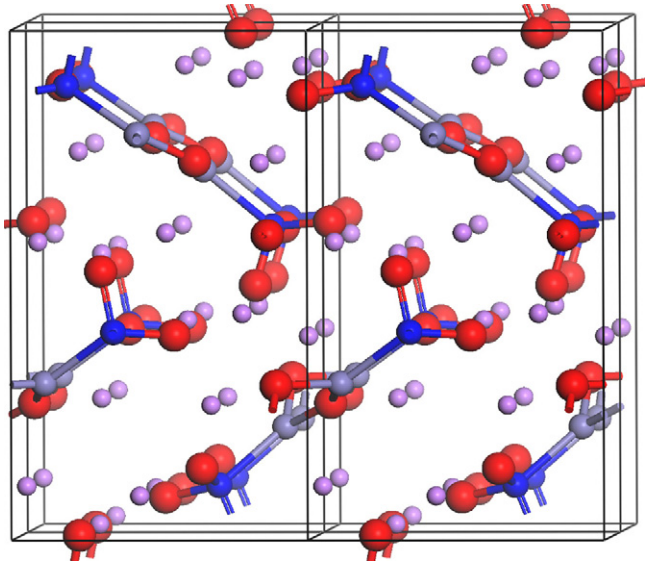

Fig. 3. Schematic view of the optimized atomic structure of Li_4FePO_4. The size and color scheme for different atoms are the same as in Fig. 1. (For interpretation of the references to color in this figure legend, the reader is referred to the web version of the article.)

4. Electronic structures and charge distributions in $Li_{1+x}FePO_4$ ($1 < x < 3$)

The electronic states of $Li_{1+x}FePO_4$ around the Fermi level are originated from the Fe 3d state, which degenerate due to two types of interactions: the crystal field and the exchange interaction. The energy gaps split by these interactions are denoted as U_{CF} (for crystal field) and U_X (for exchange interaction). The split U_X separates the spin-up and spin-down energy levels, while the U_{CF} separates the five orbits within each spin channel. In the case of $LiFePO_4$, as reported in Ref. [19], the band gap opens within the energy ranges of the minority spin channel, due to the local quasi-octahedral crystal field. As GGA calculation substantially underestimates the crystal field interactions, the calculated band gap is also underestimated. Later, GGA + U calculations improved the accuracy of the calculated band gap [24]. All the results in the present work are obtained from GGA calculations. Fortunately, although GGA always underestimate the band gap, the occupation states of the energy levels are well reproduced.

The oxidation states of Fe atoms are +2 in $LiFePO_4$, with five electrons in the majority spin channel and one electron in the t_{2g} part of minority spin channel. However, in the case of Li_2FePO_4, the oxidation states of Fe atoms become +1. There are seven electrons in the Fe 3d orbit, with five filling in the majority spin channel and two in the minority spin channel. As shown in Fig. 1c, Fe atoms are coordinated with three O atoms within the XY-plane. The planar crystal field further degenerates the Fe 3d orbital into five separate parts, z^2 and x^2–y^2 are the lowest in energy in the minority spin channel and become filled, as shown in Fig. 4. The results show that the degeneration of

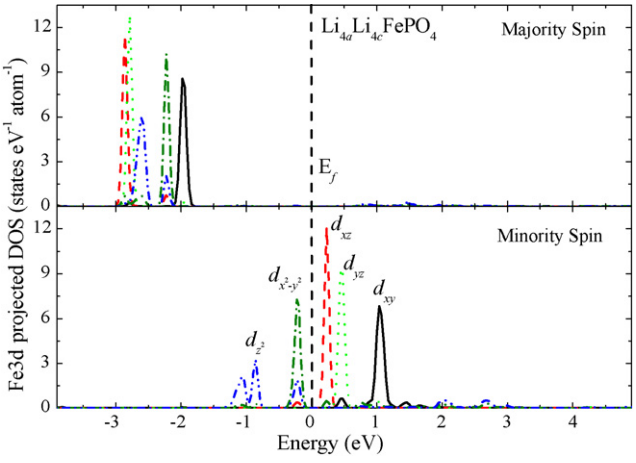

Fig. 4. Electronic density of states projected on Fe 3d orbits in $Li_{4a}Li_{4c}FePO_4$. The majority and minority spin channels are presented in the upper and lower panel, respectively. The Fermi level is aligned to 0.

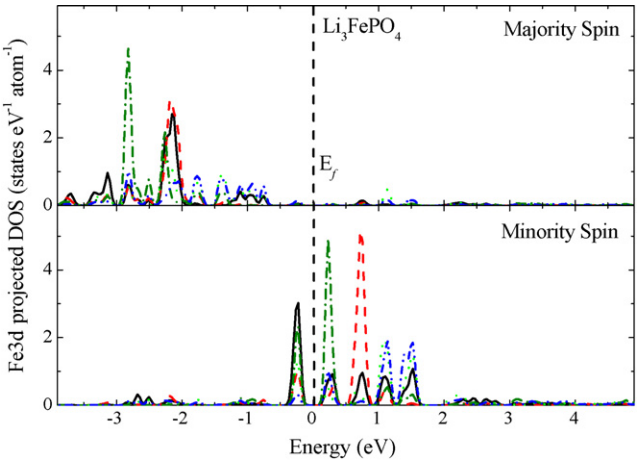

Fig. 5. Electronic density of states projected on Fe 3d orbits in Li_3FePO_4. Plot details are the same as in Fig. 4.

the Fe 3d states under the planar crystal field in the case of $Li_{4a}Li_{4c}FePO_4$ is completely different from that of under cubic crystal field as in the case of $LiFePO_4$. As more electrons take the minority spin channel, the calculated magnetic moment of Fe atom in $Li_{4a}Li_{4c}FePO_4$ is 3.03, which is smaller than that of Fe atom in $LiFePO_4$, as listed in Tables 1 and 2.

Presented in Fig. 5 is the electron DOS projected on Fe 3d orbits in Li_3FePO_4. From the crystal structure of Li_3FePO_4, Fe atom is connected with one P and two oxygen atoms. The arrangement of Fe, O, and P atoms is not symmetric to *x*-, *y*- or *z*-axis in the unit cell. The DOS projected on Fe 3d orbits cannot be clearly separated. However, we can see that the occupation of the minority spin channel is quite low, which indicates that Fe atoms do not collect much charge after Li atoms are intercalated into the Li_2FePO_4 lattice and become Li_3FePO_4.

To understand the electronic structure of Li_2FePO_4 and Li_3FePO_4, it is necessary to know the charge distributions in the lattice. That is to say, we need to know when lithium atoms are added into the lattice, how the charge is redistributed within the lattice. For this purpose, we calculated the differential charge density ρ_{diff}, which is defined as the difference between charge density of $\rho[Li_xFePO_4]$ and $\rho[Li_{\square}FePO_4]$. Here $\rho[Li_{\square}FePO_4]$ denotes the charge density after removing all Li atoms from Li_xFePO_4 without relaxing the atomic positions. By analyzing such a plot, it can be seen clearly where the charge from the Li atoms goes, as shown in Fig. 6. In all cases, Li atoms are completely ionized and in the form of Li^+. In $LiFePO_4$, the charge from Li atoms is mainly collected by Fe atoms, and thus the oxidation state of Fe becomes +2 (see Fig. 6a). For the case of $Li_{4a}Li_{4b}FePO_4$, however, Fe atoms do not collect much share; the majority part of the charge from Li atoms is collected by O atoms that do not belong to members of the ring (see the crystal structure in Fig. 1b). Situation for the case of $Li_{4a}Li_{4c}FePO_4$ is also different, in which the charge is mainly collected by Fe atoms, and filled into the z^2 and $x^2–y^2$ orbits. As shown in Fig. 6d for the case of Li_3FePO_4, both Fe and O atoms collected some charge. Those O atoms that bonded with P atoms get even more share than those connected with Fe atoms. Charge redistribution is accompanied by the structural changes, during the Li intercalation process.

5. Migration of Li ions in Li_3FePO_4

It is reported that lithium diffusions in $LiFePO_4$ is one-dimensional, which is partly responsible for the poor rate performance of the material as cathode for lithium ion batteries [5,7]. However, the situation is quite different for $LiFePO_4$ as anode material. We show in this part that migration of Li ions in the chained structure Li_3FePO_4 is three-dimensional. For the convenience of comparison, we first calculated the energy barrier of lithium diffusion in the one-dimensional pathway in $LiFePO_4$. The energy barrier calculated with NEB method is 0.29 eV in the present work, which is in good agreement with Ref. [5].

Fig. 7 presents the migration pathway and energy barriers for lithium diffusion in the chained Li_3FePO_4. Five Li sites are marked by numbers from 1 to 5 in the unit cell, as shown on the left side of Fig. 7. There are four diffusion pathways are simulated: from site 1 to site 2 (denote as 1–2 and see Fig. 7a), site 1 to site 4 (denote as 1–4 and see Fig. 7b), site 1 to site 3 (denote as 1–3 and see Fig. 7c) and site 4 to site 5 (denote as

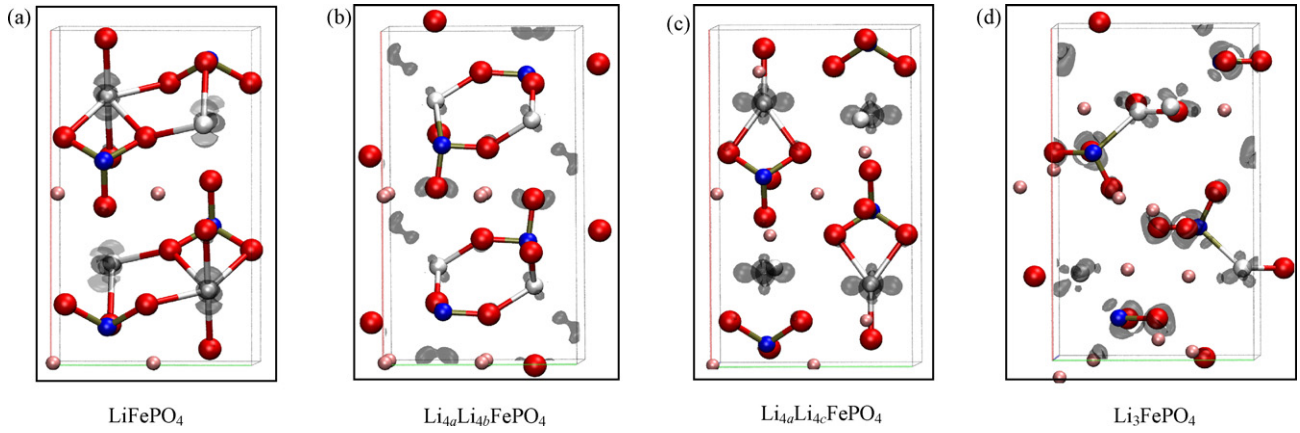

Fig. 6. Differential charge density $\rho_{diff} = \rho[Li_xFePO_4] - \rho[Li_{\square}FePO_4]$ for (a) $LiFePO_4$, (b) $Li_{4a}Li_{4b}FePO_4$, (c) $Li_{4a}Li_{4c}FePO_4$, and (d) Li_3FePO_4. The color and size scheme for different atoms are the same as in Fig. 1, the isosurfaces of the differential charge density are in black and transparent. (For interpretation of the references to color in this figure legend, the reader is referred to the web version of the article.)

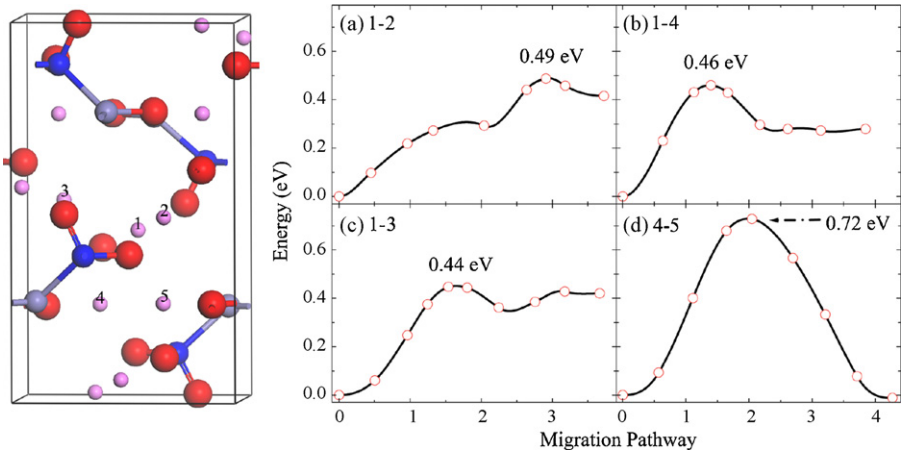

Fig. 7. Migration energy barrier for Li ions diffusion in chained Li_3FePO_4 along different migration pathway. The numbers 1–5 refer to five Li sites in the lattice.

4–5 and see Fig. 7d). Migration pathways of 1–2 and 4–5 are migration of Li ions between different chains, while migration pathways of 1–3 and 1–4 are migration of Li ions within a chain. Although the calculated energy barriers (0.49, 0.46, 0.44, and 0.72 eV for 1–2, 1–4, 1–3, and 4–5, respectively) are a little larger than the energy barrier (0.29 eV) of lithium ions diffusion along the one-dimensional pathway in $LiFePO_4$, they do not differ very much from each other. This shows that lithium ions diffusion in Li_3FePO_4 is three-dimensional. Furthermore, lithium diffusion from one chain to another is more difficult than migration within a chain, as the energy barrier is a little larger for lithium migration from one chain to another.

6. Summary and conclusions

In summary, $Li_{1+x}FePO_4$ ($1 \leq x \leq 3$) as anode material for lithium ion batteries has been investigated using *ab initio* calculations. Large structure changes accompanying large volume expansions are observed when first two Mole lithium atoms are intercalated into the $LiFePO_4$ lattice. Then the final product of Li_3FePO_4 possesses a chained structure, which is quite stable and in favor of lithium storage and migration. Upon additional lithium atoms intercalated into the Li_3FePO_4 chained structure, the chained structure keeps unchanged and the cell volume expansion is very small. Within the chained structure, lithium diffusions are in a three-dimensional pathway, which is different to the one-dimensional pathway in $LiFePO_4$ as cathode material.

Acknowledgments

Thanks to the support of NSFC under Grant Nos. 10604023 and 10564002, and Science Foundation of department of Education of Jiangxi province under Grant No. [2007]121 and Zhejiang Sci-Tech University (ZSTU) under Grant No. 0613271-Y. Calculations were partially performed at the central computational facilities of the Ecole Polytechnique Fédéral de Lausanne (EPFL).

References

[1] K. Padhi, K.S. Nanjundaswamy, J.B. Goodenough, J. Electrochem. Soc. 144 (1997) 1188.
[2] S.Y. Chung, J. Bloking, Y.M. Chiang, Nat. Mater. 1 (2002) 123.
[3] S.Q. Shi, L.J. Liu, C.Y. Ouyang, D.S. Wang, Z.X. Wang, L.Q. Chen, X.J. Huang, Phys. Rev. B 68 (2003) 195108.
[4] C.Y. Ouyang, S.Q. Shi, Z.X. Wang, H. Li, X.J. Huang, L.Q. Chen, J. Phys.: Condens. Mat. 16 (2004) 2265.
[5] D. Morgan, A. Van der Ven, G. Ceder, Electrochem. Solid-State Lett. 7 (2004) A30.
[6] T. Maxisch, F. Zhou, G. Ceder, Phys. Rev. B 73 (2006) 104301.
[7] C.Y. Ouyang, S.Q. Shi, Z.X. Wang, H. Li, X.J. Huang, L.Q. Chen, Phys. Rev. B 69 (2004) 104303.
[8] S. Franger, F. Cras, C. Bourbon, H. Rouault, Electrochem. Solid-State Lett. 5 (2002) A231.
[9] H. Huang, S.C. Yin, F. Nazar, Electrochem. Solid-State Lett. 4 (2001) A170.
[10] N. Kalaiselvi, C.H. Doh, C.W. Park, S.I. Moon, M.S. Yun, Electrochem. Commun. 6 (2004) 1110.
[11] N. Jayaprakash, N. Kalaiselvi, Electrochem. Commun. 9 (2007) 620.
[12] Free software developed by B. Hammer et al., for details please refer to: https://wiki.fysik.dtu.dk/dacapo.
[13] M.C. Payne, M.P. Teter, D.C. Allan, T.A. Arias, J.D. Joannopoulos, Rev. Mod. Phys. 64 (1992) 1045.
[14] D. Vanderbilt, Phys. Rev. B 41 (1990) R7892.
[15] J.P. Perdew, J.A. Chevary, S.H. Vosko, K.A. Jackson, M.R. Pederson, D.J. Singh, C. Fiolhais, Phys. Rev. B 46 (1992) 6671.
[16] H.J. Monkhorst, J.D. Pack, Phys. Rev. B 13 (1976) 5188.
[17] G. Henkelman, H. Jonsson, J. Chem. Phys. 113 (2000) 9978.
[18] G. Henkelman, B.P. Uberuaga, H. Jonsson, J. Chem. Phys. 113 (2000) 9901.
[19] S.Q. Shi, C.Y. Ouyang, D.S. Wang, Z.X. Wang, L.Q. Chen, X.J. Huang, Phys. Rev. B 71 (2005) 144404.
[20] M. Yonemura, A. Yamada, Y. Takei, N. Sonoyama, R. Kanno, J. Electrochem. Soc. 151 (2004) A1352.
[21] P. Poizot, S. Laruelle, S. Grugeon, L. Dupont, J.M. Tarascon, Nature 407 (2000) 496.
[22] P. Balaya, H. Li, L. Kienle, J. Maier, Adv. Funct. Mater. 13 (2003) 621.
[23] Y.S. Hu, Y.G. Guo, W. Sigle, S. Hore, P. Balaya, J. Maier, Nat. Mater. 5 (2006) 713.
[24] F. Zhou, K. Kang, T. Maxisch, G. Ceder, D. Morgan, Solid-State Commun. 132 (2004) 181.